

Design of a Wideband, 100 Watt, 140 GHz Gyroklystron Amplifier

Colin D. Joye*

Massachusetts Institute of Technology

(Dated: October 27, 2004)

The design study of a 140 GHz, 100 W continuous wave gyroklystron amplifier is presented. The device is intended for use in Dynamic Nuclear Polarization enhanced Nuclear Magnetic Resonance (DNP/NMR) spectroscopy experiments. The gyroklystron has five cavities and operates in the TE(0,2) mode with a low power electron beam. The design was performed using MAGY, a nonlinear code for modeling gyro-devices. The gyroklystron design process starting from the linear theory to the optimization of the final design in MAGY has been described in detail. Stagger tuning was employed to broadband the device. The design yields 130 W peak power, 36 dB saturated gain, and a -3 dB bandwidth of over 1 GHz (0.75%) with a 15 kV, 150 mA electron beam having a beam pitch factor of 1.5, radius of 0.64 mm and calculated perpendicular momentum spread of 4%. Preliminary designs of the Magnetron Injection Gun (MIG), the input and output couplers, and the mode converter to transform the TE(0,2) operating mode to the HE(1,1) mode for low loss transmission of the output power are also presented. The design meets the specifications for the DNP experiment.

I. INTRODUCTION

A wideband, 140 GHz, 100 Watt continuous wave amplifier is required for Dynamic Nuclear Polarization (DNP) enhanced Nuclear Magnetic Resonance (NMR) spectroscopy experiments in the Francis Bitter Magnet Laboratory (FBML) at the Massachusetts Institute of Technology, Cambridge, MA. In order to increase the Signal-To-Noise (SNR) ratio of the spectroscopy process, the sample is polarized by electromagnetic radiation introduced into the DNP probe [1]. SNR enhancement factors on the order of several hundred are possible using this technique [2]. For flexibility during this process, it is desirable that the amplifier sourcing this radiation be capable of continuous wave (CW) operation as well as short pulses on the nanosecond scale.

The gyro-amplifier is a promising technology that can be used to meet this goal. Gyro-amplifiers typically consist of a high quality electron beam that is guided by a precision magnetic field through either a series of cavities or a straight, lossy traveling wave section. The former is termed a gyroklystron, while the latter is called the gyro-Traveling Wave Tube (gyro-TWT). Hybrids consisting of a traveling wave section and a series of cavities are also possible. An electromagnetic wave (referred to as simply "RF") of low power is coupled into the amplifier at the input end of the tube circuit. It is then amplified through an interaction with the electron beam and extracted from the output end of the circuit.

In gyro-devices, the Cyclotron Resonance Maser (CRM) interaction takes place between the transverse electric fields in the cavity and the transverse velocity component of the electrons as they gyrate around the magnetic field lines. Because this interaction is due to the transverse electric fields, only the TE_{mn} modes are

considered as possible operating modes in the cavity circuits.

The choice of the gyroklystron over the gyro-TWT was made based on many factors. Gyro-TWTs are capable of very high gain and very wide bandwidth because they consist most simply of a long, straight, non-resonant interaction structure [3]. The gyro-TWT, however, has not been demonstrated at power levels as low as those proposed here, because the bandwidth and gain rapidly deteriorate at low beam currents. The gain of the gyro-TWT is typically increased either by raising the beam current or by increasing the interaction circuit length. The latter of these two may not even be possible because of the sensitivity in the gyro-TWT to velocity spread in the electron beam. Gyro-TWTs are also notorious for problems with self-oscillation due to a plethora of undesired backward-propagating modes [4], a problem that worsens as the beam current increases. Gyroklystrons, however, promise high gain per cavity, low noise and moderate bandwidth and are generally less vulnerable to self-oscillations. While the gain of the gyroklystron is also severely limited by low beam current, it is possible to compensate to some degree by changing the characteristics of the individual cavities. Furthermore, by employing the method of stagger tuning, the bandwidth of the gyroklystron can be widened at the expense of gain [5].

Recently demonstrated gyroklystrons include: A 94 GHz gyroklystron with a 10 kW average output power and a 700 MHz (0.74%) bandwidth [6]; a 94 GHz gyroklystron with 410 MHz (0.44%) bandwidth and 50 dB of saturated gain [7]; and an extremely high power 100 MW, Ku-band gyroklystron [8]. A sub-millimeter wavelength, 1 kW, 360 GHz second harmonic gyroklystron with a 70 MHz (0.02%) bandwidth has also been designed [9].

This paper describes the design of a 140 GHz, 100 W gyroklystron amplifier with a -3 dB bandwidth of over 1 GHz (0.75%), operating with a saturated gain of 36 dB. These design goals were achieved using an electron beam

*cjoye@mit.edu

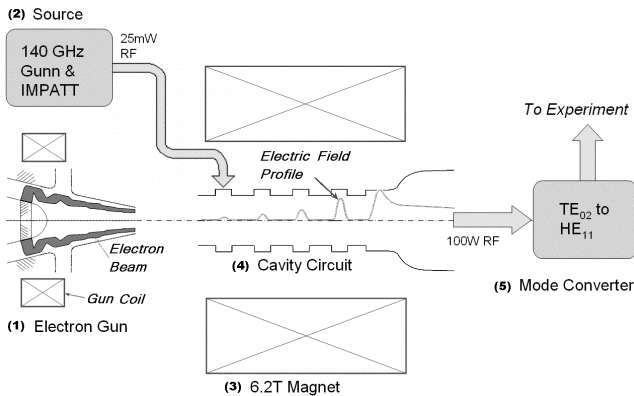


FIG. 1: The gyrokystron block diagram: (1) Electron gun (MIG); (2) Solid state low power RF source; (3) Superconducting magnet; (4) Cavity circuit; (5) Mode converter.

voltage of only 15 kV and a beam current of only 0.15 A. The use of such an unusually low beam power was desirable in order to keep the efficiency to a reasonable value of around 5.7%.

The presentation of this material is organized as follows: First, a brief overview of the project is presented, followed by the details of the design work including the cavity circuit, mode converter, electron gun and preliminary input coupler. In the final section, concluding remarks are given.

II. OVERVIEW

The system block diagram for the gyrokystron is shown in Fig. 1. The hollow, annular electron beam is emitted by the indirectly heated cathode of a Magnetron Injection Gun (MIG) at one extreme of the tube. This beam is guided through the cavity circuit by a solenoidal magnetic field with a peak value of approximately 5.2 Tesla centered in the interaction region. After the electron beam exits the cavity circuit, it is then collected at the other extreme of the tube by a water cooled collector (not shown).

The gyrokystron cavity circuit consists of an alternating series of resonant cavities and cut-off drift spaces. In the first cavity, RF power is coupled in from the external source. As the electron beam enters the first cavity, the RF electric field produces a force on the electrons as they spiral around the magnetic field lines. This force not only changes the phase of the electrons as their orbits are slowed down and sped up, but it also causes the electrons to emit bremsstrahlung radiation, which is superimposed over the existing fields in the cavity. This effect of changing the transverse momentum of the electrons by interaction with an electric field leads to a process called bunching, which causes a majority of the electrons to emit bremsstrahlung radiation in phase coherently.

After the first cavity, the electron beam enters a cutoff region called the drift space where the electromagnetic

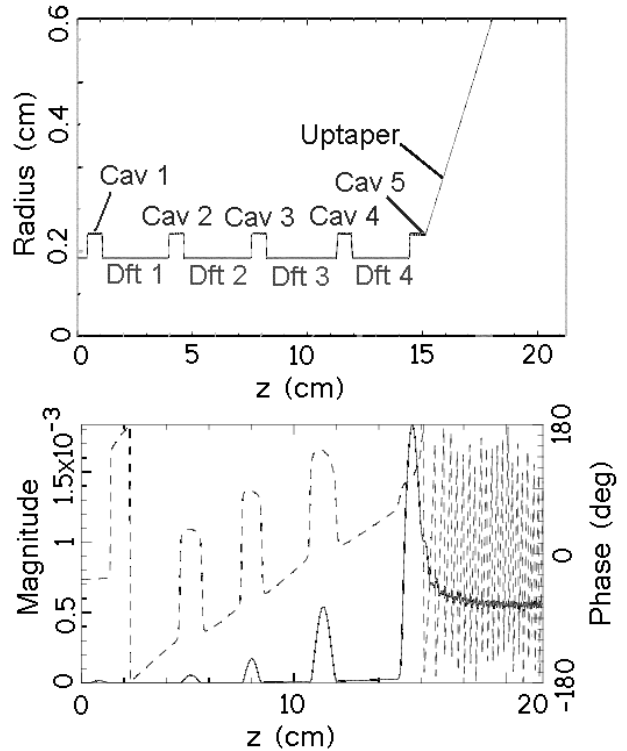


FIG. 2: The layout of the gyrokystron cavity circuit consisting of five cavities separated by four drift spaces and an uptaper section (top); Evolution of the electric field magnitude (solid line) and phase (dashed line) in the cavities (bottom).

fields are evanescent (Fig. 2). The electron phases, being affected by the RF-induced forces in the first cavity, continue to evolve in the drift space in a process known as ballistic bunching. Upon entering the second cavity, where no pre-existing RF is present, the electrons radiate RF at a frequency close to the Doppler-shifted cyclotron frequency given by the intersection of the beam line of the fast cyclotron mode and the dispersion curve of the structure. If the cavity is tuned properly, the bunching in the beam will be reinforced and the total RF fields in the second cavity will be higher than those in the first cavity. This process continues until the last (fifth) cavity, where the RF energy is extracted from the beam, allowed to travel through the uptaper section and then converted from the TE_{02} operating mode to HE_{11} mode in three steps: TE_{02} to TE_{01} using a rippled wall mode converter; TE_{01} to TE_{11} using another rippled wall mode converter; and TE_{11} to HE_{11} using a scalar horn. The latter two mode conversion steps are already part of the existing DNP experiment. After the mode converters, the power is finally sent to the DNP probe by means of a low loss, overmoded waveguide.

III. DESIGN

Several major challenges arise when designing such a high frequency, low beam power gyrokystron. There are unfavorable scaling laws associated with high frequency [10]: Magnetic field scales with frequency, so superconducting magnets are required above 30 GHz or so unless cyclotron frequency harmonics are utilized; the ohmic losses tend to increase with frequency due to the skin depth effect; and the cavity dimensions scale inversely with frequency for a fixed mode. This latter scaling law means high frequency gyro-amplifiers must have proportionally tighter tolerances in the fabrication of proportionally smaller cavities unless a higher order mode is used. Ohmic heating becomes an important factor due to the smaller cavity wall surface areas at high frequencies and due to the ohmic losses. At low beam current, the gain falls off rapidly, requiring an increase in the cavity ohmic Q -factors, which makes the system inherently more narrow band. Alternatively, the lowering of the ohmic Q -factors can be compensated for to some degree if the cavity lengths are increased; but this method increases the detrimental consequences of velocity spread. All of these tradeoffs must be carefully considered at high frequencies.

Typical values for a five-cavity, high power gyrokystron in the W-band (94 GHz) might be a 50 kV, 5 A electron beam with cavity ohmic Q -factors on the order of 100 for the input and prebuncher cavities and 300 for the output cavity, with cavity lengths of no more than $3\lambda_0$, where λ_0 is the free space wavelength at the center frequency. One might expect a peak power of around 50 kW with a 500 MHz bandwidth and a linear gain of maybe 50 dB from such a device. In scaling to lower beam powers, problems with space charge in the electron gun design were found due to low beam voltage, so the minimum voltage was limited to around 15 kV. To maintain reasonable efficiency, a 1 kW beam power was chosen as the starting point, which meant that the beam current would be only 0.07 A. Eventually, simulations including velocity spread showed that the requirements for gain and bandwidth could not be met with such a low beam current, so the value was increased to 0.15 A. The higher value of beam current provided enough gain that even stronger stagger tuning could be used for wider bandwidth.

A. Linear Theory

The first step taken in the design of the gyrokystron circuit was to study the linear theory [11]. In the linear regime, the small-signal gain is obtained by ignoring the nonlinear effects of saturation. The linear theory is typically a good approximation for all cavities except the final cavity, where the nonlinear theory becomes important.

Analysis of gyro-devices can be carried out using a set of normalized variables. The normalized field amplitude

in the cavity is defined to be F , the normalized length of the cavity is μ , and Δ is the detuning parameter defined by

$$\mu = \frac{\pi\beta_{\perp 0}^2 L}{\beta_{\parallel 0} \lambda} \quad (1a)$$

$$F = \frac{E_0\beta_{\perp 0}^{n-4}}{B_0 c} \left(\frac{n^{n-1}}{2^{n-1}n!} \right) J_{m\pm n}(k_{\perp}r_b) \quad (1b)$$

$$\Delta = \frac{2}{\beta_{\perp 0}^2} \left(1 - \frac{n\omega_{c0}}{\omega} \right) \quad (1c)$$

where $\beta_{\parallel} = v_{\parallel}/c$ and $\beta_{\perp} = v_{\perp}/c$ are the normalized electron velocity components, L is the length of the cavity, n is the harmonic index (which will be assumed to be unity from here on), $\omega_c = eB_0/\gamma_0 m_e$ is the cyclotron frequency, r_b is the radius of the electron beam and the subscript “0” denotes quantities at the entrance of the interaction region. The plus and minus signs on the Bessel function indicate asymmetric modes ($m \neq 0$) rotating in the same or opposite direction as the spiraling electrons, respectively. For a cylindrical cavity supporting the TE_{0p} azimuthally symmetric cylindrical waveguide mode, the field amplitude E_0 is calculated by integrating over the fields to obtain the energy. This equation, along with the equation for total Q , allows us to find E_0 for a sinusoidal axial profile, which is used for the input cavity,

$$E_0 = \sqrt{\frac{Q_{tot(1)}P_{in}}{\omega\epsilon_0\pi L} \frac{2}{r_c|J_0(\nu_{0p})|}} \quad (2)$$

where P_{in} is the input power to the first cavity, and Q_{tot} is defined as,

$$\frac{1}{Q_{tot}} = \frac{1}{Q_{ohmic}} + \frac{1}{Q_{diffractive}} \quad (3)$$

Now we can look at the governing equations of momentum for the electrons. Under the assumption of a single-mode fundamental interaction and an approximation of weakly relativistic electrons ($\beta_{\perp}^2 \ll 2$), the equations of motion reduce to the so-called Yulpatov pendulum equations [12],

$$\frac{dp}{d\zeta} = -Ff(\zeta)\sin\theta \quad (4a)$$

$$\frac{d\theta}{d\zeta} = -(\Delta + p^2 - 1) - Ff(\zeta)p^{-1}\cos\theta \quad (4b)$$

where p is the normalized momentum, θ is the momentum phase angle and ζ is the normalized axial distance,

$$p = \frac{\gamma\beta_{\perp}}{\gamma_0\beta_{\perp 0}} \quad (5a)$$

$$\theta = \phi - \omega t_0 + \frac{\pi}{2} \quad (5b)$$

$$\zeta = \frac{\pi\beta_{\perp 0}^2 z}{\beta_{\parallel 0} \lambda} \quad (5c)$$

where ϕ is the fast time scale phase angle of the electron, t_0 is the time when the electrons enter the interaction region, and $\gamma_0 \simeq 1 + V_0(kV)/511$. $p(\zeta_{in}) = 1$ is the normalized input momentum (assuming no velocity spread) and $\theta(\zeta_{in}) = \theta_0$, where θ_0 is uniformly distributed over $[0, 2\pi)$. In the final cavity, $\zeta_{in} = -\sqrt{3}\mu/2$ and $\zeta_{out} = \sqrt{3}\mu/2$ are typically chosen as the normalized input and output distances because they approximate gyrotron tapered resonators well.

The $f(z)$ term in Eqs. 4 are typically chosen to be a Gaussian field profile or a sinusoidal field profile. The Gaussian profile is used in the extraction cavity (last cavity) where the field leaks out toward the tube output. The sinusoidal profile goes to zero at $\zeta = \{0, \mu\}$ and so is used for closed cavities. The forms are as follows,

$$f(\zeta) = e^{-\left(\frac{2\zeta}{\mu}\right)^2} \quad (6a)$$

$$f(\zeta) = \sin\left(\frac{\pi\zeta}{\mu}\right) \quad (6b)$$

Using perturbation theory by expanding the momentum p and phase θ in the limit of small F parameter, we can linearize the pendulum equations presented in Eqs. 4 for a simple two-cavity gyrokystron as follows,

$$p = p^{(0)} + p^{(1)} + \dots \quad (7a)$$

$$\theta = \theta^{(0)} + \theta^{(1)} + \dots \quad (7b)$$

the equations become,

$$\frac{dp^{(0)}}{d\zeta} = 0, \quad (8a)$$

$$\frac{d\theta^{(0)}}{d\zeta} = -(\Delta + p^{(0)2} - 1), \quad (8b)$$

$$\frac{dp^{(1)}}{d\zeta} = -Ff(\zeta)\sin\theta^{(0)}, \quad (8c)$$

$$\frac{d\theta^{(1)}}{d\zeta} = -2p^{(0)}p^{(1)} - \frac{Ff(\zeta)\cos\theta^{(0)}}{p^{(0)}}, \quad \dots \quad (8d)$$

Solving these equations, integrating, approximating the result and making the assumptions that $|\mu x - 1| \ll 1$ and that there is no field in the drift spaces ($F = 0$), the analysis presented in [11] generalizes to an N -cavity gyrokystron as follows,

$$F_j = \frac{\sqrt{\pi}}{2} \hat{I} \mu_j e^{-x_j^2} q_{j-1} (1 + \delta_j^2)^{-1/2}, \quad (9a)$$

$$\frac{q_j}{q_{j-1}} = \frac{\pi}{2} \hat{I} \mu_j^2 \hat{\mu}_{d,j} e^{-2x_j^2} (1 + \delta_j^2)^{-1/2}, \quad j = 2, \dots, N-1 \quad (9b)$$

for j^{th} normalized cavity length μ_j and parameter $\hat{\mu}_{d,j}$, detuning parameter Δ_j , parameter $x = \mu\Delta/4$ and frequency pulling parameter $\delta_j = 2(\omega - \omega_0)Q_0/\omega$, where Q_0 and ω_0 characterize the unloaded cavity and ω is the working frequency in the loaded cavity. The variable $\hat{\mu}_{d,j}$

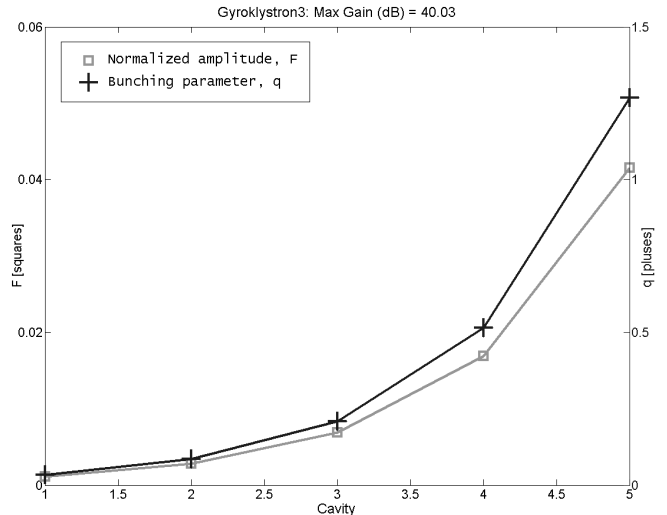


FIG. 3: The result of the linear code showing the evolution of F and q values corresponding to about 40 dB of linear gain.

contains the normalized j^{th} drift space length $\mu_{d,j}$,

$$\hat{\mu}_{d,j} = \frac{\sqrt{3}}{2} \mu_j + \mu_{d,j}, \quad (10)$$

and the normalized current \hat{I} is given by,

$$\hat{I} = \left(\frac{\sqrt{2}}{\pi^{5/2}} \right) \frac{I_A Q_{tot}}{c^3 m_e \epsilon_0 / e} \frac{\beta_{\perp 0}^{-4}}{\gamma_0} \frac{\lambda}{L} \frac{J_{m\pm 1}^2(k_{\perp} r_b)}{(\nu_{mp}^2 - m^2) J_m^2(\nu_{mp})} \quad (11)$$

where I_A is the actual beam current in amps. The constant $(\sqrt{2}/\pi^{5/2})$ in front of Eq. 11 is for a Gaussian profile. It becomes simply (π^{-2}) for a sinusoidal profile.

In using these equations, the q parameter is calculated in the first cavity by,

$$q_1 = \sqrt{\pi} F_1 \mu_1 e^{-x_1^2} \hat{\mu}_{d,1} \quad (12)$$

and F_1 was calculated using Eqs. 1b and 2. The F and q values for the other cavities were then calculated in an iterative manner through Eqs. 9, producing Fig. 3, which corresponds to a five-cavity gyrokystron with a predicted linear gain of 40 dB using cavity lengths of $3.5\lambda_0$ with total Q -factors of 1000 each and a 15 kV, 0.065 A beam with a pitch factor of $\alpha = 1.5$ and a 15 mW input power. The drift spaces were each $8.0\lambda_0$ long and the effects of velocity spread were not included. The linear theory is approximately valid for $q < 0.7$, which corresponds to all but the final cavity in the figure, as expected.

It was expected that 25 mW of input power could be coupled into the first cavity, so 40 dB of linear gain was desired to reach the above the 100 W level at saturated output. These results were used to set the starting point for the nonlinear, self-consistent gyrokystron simulation that was carried out using the established MAGY [13] code.

B. Circuit Simulation

MAGY can be used for nonlinear, time dependent modeling of slow and fast wave microwave devices that are axially symmetric and utilize an electron beam. The electromagnetic field amplitudes are calculated using a small number of coupled, one-dimensional differential equations instead of the full solution to Maxwell's equations. The time scale used is the fill time of the cavity instead of the cyclotron frequency, and the guiding center approximation is used to solve the electromagnetic fields as driving forces. It calculates the self-consistent fields for the electrons by using the electrons as current sources for the fields at each time step. It is a well-established code in the field of gyro-devices.

The strategy used to perform this design was to maximize the electric field strength in each cavity following the direction of the electron beam traversal, *i.e.*, the first cavity radius was perturbed and the radius corresponding to the highest electric field was saved. Next, the cavity length was perturbed followed by the drift space length and the second cavity radius, and so on. At each step, the values were saved that corresponded to the peak electric field in the cavity being perturbed. This process starting from the first cavity all the way to the end of the linear uptaper was repeated many times before the output power finally reached a maximum. This method tended to result in zero stagger tuning, so once the design began to converge, the gain tended to saturate and then over-saturate due to excess gain.

After reaching a maximum output power at the center frequency, a sweep of the frequency in MAGY simulations showed that the bandwidth was no where near the desired 1 GHz (0.75%) mark. To widen the bandwidth, the concept of stagger tuning was used by detuning the cavities [14]. Some cavities were tuned higher than the center frequency and others were tuned lower, with a final difference of 1.6 GHz (1.2%) between the highest and lowest frequencies. Several frequency tuning patterns were attempted until a pattern began to produce the desired result. Once a pattern was established, the iterative optimization process continued as before, but with the goal of pushing both power and bandwidth upward. The cavity resonant frequencies were continually adjusted to maintain a good balance between power and bandwidth. In order to meet the specifications, it was necessary to use an aggressive stagger tuning that was obtained at the expense of gain. To bring the linear gain back up to the desired value of 40 dB, the cavity ohmic Q -factors, cavity lengths and drift space lengths were all increased in careful balance.

There were many tradeoffs involved in this optimization. Increasing the Q -factors or cavities lengths lowers the critical oscillation start current, which should be kept at least a factor of two above the beam current. Increasing the cavity or drift space lengths increases the detrimental effect of velocity spread. Increasing the Q -factor can decrease the bandwidth if it is too high. Simulations

TABLE I: Final Design Parameters

Operation Voltage, V_0	15 kV
Beam Current, I_0	0.15 A
Pitch factor $\alpha = v_{\perp}/v_{\parallel}$	1.5
Perpendicular velocity spread	4 %
Design Mode	TE_{02}
Input Power, P_{in}	25 mW
Magnetic Field, B_0	5.14 T
Output Power	130 W
Efficiency	5.7%
-3 dB Bandwidth	1050 MHz
Bandwidth at 50W	1270 MHz
Saturated Gain	36 dB

	Length(λ_0)	Radius(mm)	f_0 (GHz)	Q_{ohm}	Q_{diff}
cav1	3.73	2.400	140.02	500	800
dft1	16.1	1.85			
cav2	4.20	2.417	139.04	750	
dft2	9.33	1.85			
cav3	3.73	2.423	138.70	700	
dft3	11.2	1.85			
cav4	5.37	2.413	139.27	400	
dft4	14.5	1.85			
cav5	4.53	2.394	140.37	1700	360
uptaper	17.7				
straight	12.6	4.0			

were performed with these tradeoffs in mind along with careful tuning of the cavities until the desired result was achieved.

In the MAGY code, the ohmic Q -factors are chosen at will by the user, while in fabrication it is impractical to lower the conductivity of the fabrication material. After the design is finalized, a common treatment is to simulate the loading of the cavities with carefully designed lossy ceramic rings to provide ohmic loss. The cavity dimensions may have to be altered slightly to maintain the correct tuning frequencies. Other methods for lowering the ohmic Q exist, such as the use of slots in the cavity wall that would allow power to diffract out and be absorbed outside of the cavity. This method may even allow the ohmic Q -factors to be tuned after assembly.

In raising the cavity ohmic Q -factors, it was found that there is a side benefit to excess gain in that the center frequency begins to reach a moderately saturated maximum power while the sidebands continue to receive more linear gain. In this manner, the bandwidth and gain can simultaneously increase, as in Fig. 4 where the ohmic Q -factor of the third cavity was varied keeping all other parameters fixed. In this particular cavity, it is evident that both power and bandwidth increase steadily up to $Q_3 \approx 600$, where the bandwidth reaches a maximum. Due to this phenomenon, the final cavity Q -factors could

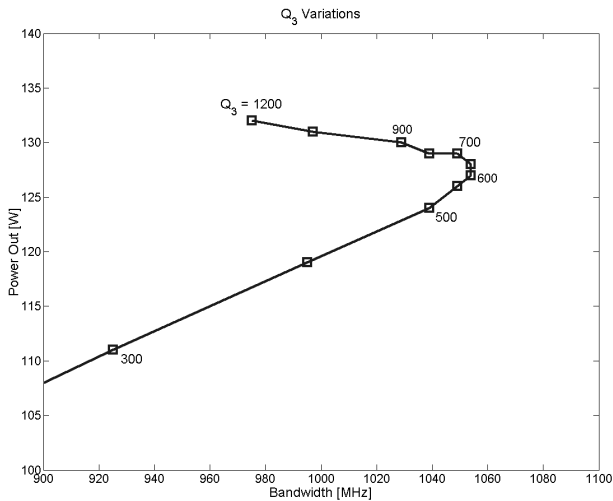


FIG. 4: Power and bandwidth can simultaneously increase by increasing the ohmic Q -factor over a limited range by use of moderate saturation (third cavity perturbed). The design value was $Q_3 = 700$.

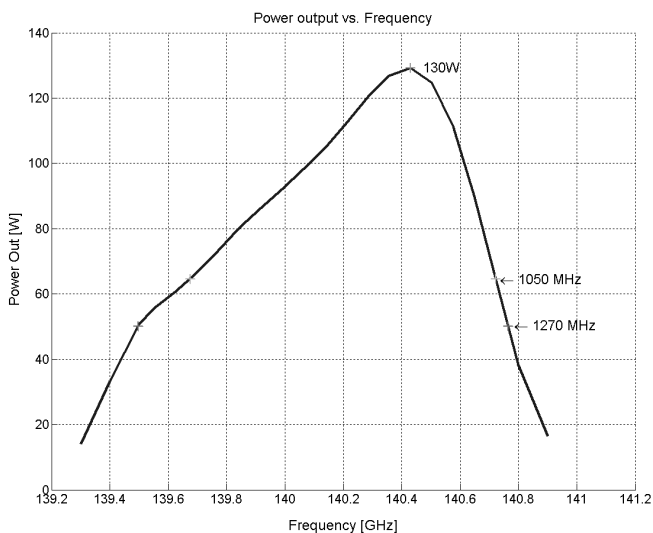


FIG. 5: The frequency response for the final gyrokystron design with an input power of 25 mW and design parameters in Tab. I.

thus be higher than originally expected. In high power gyrokystrons, where the beam current to beam voltage ratio is typically much higher, this regime is risky because the critical oscillation start current is a strong function of both the Q -factor and the beam current.

After many iterations of using MAGY to optimize the gyrokystron circuit, the design goals were finally met. The results gave a maximum output power of 130 W with just over 1 GHz of -3 dB bandwidth and almost 1.3 GHz of bandwidth available at the 50 W level, which is the -3 dB power level for a 100 W maximum device that just meets the specifications (Fig. 5). Tab. I shows the final operation parameters and cavity specifications

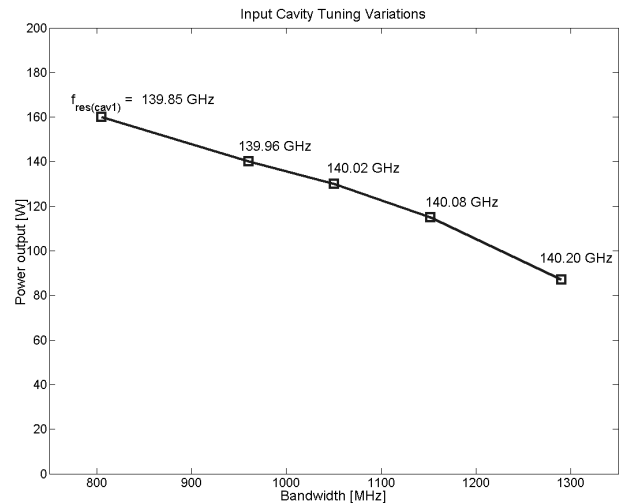


FIG. 6: The tradeoff between power and bandwidth for various input cavity tunings. The design value was 140.02 GHz.

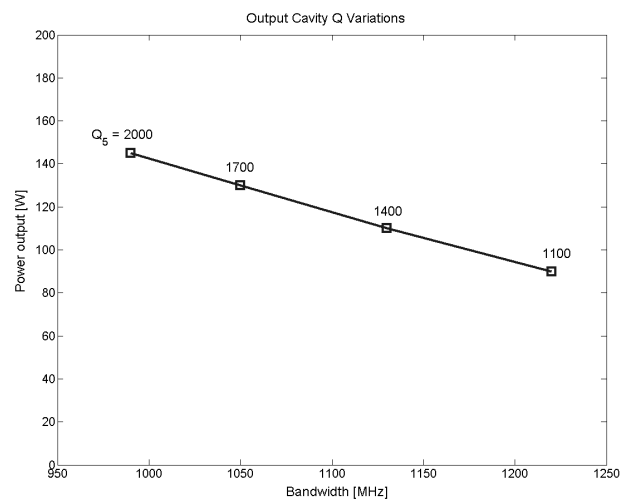


FIG. 7: The tradeoff between power and bandwidth for various values of the ohmic Q -factor for the last cavity. The design value was 1700.

along with the results.

Holding all other design parameters constant, Fig. 6 was generated to show the effect on power and bandwidth of detuning the first cavity cold resonant frequency from the final design value of 140.02 GHz. Errors in tuning of only about 40 MHz lead to deviations in bandwidth and power of approximately 10%. In fabricating such a cavity, even electroforming can only guarantee an accuracy of about 300 MHz, so it may be necessary to provide some means for manual tuning to correct the resonant frequencies during cold testing. A cold test of the fabricated cavities would yield the actual Q -factors and resonant frequencies of each cavity. This data would be used to simulate the performance of the gyrokystron as fabricated. Necessary tuning and Q -factor adjustments would be made at that time.

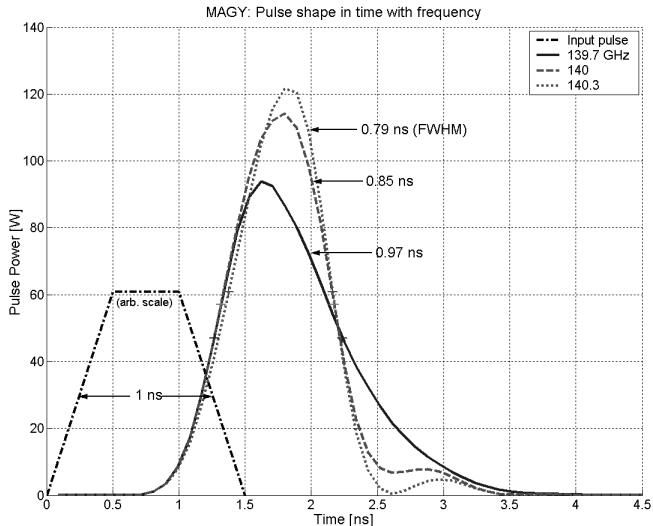


FIG. 8: Output short pulses for a 1 ns wide input pulse (FWHM) at 139.7 GHz, 140.0 GHz and 140.3 GHz carrier frequencies.

In Fig. 7, the output cavity ohmic Q -factor was adjusted to show the power to bandwidth tradeoff. For this figure all other design parameters were again held constant. The simulation exhibits the expected behavior. The predicted pulse shapes are also quite good for a 1 ns wide (FWHM) pulse, as shown in Fig. 8.

C. Uptaper and Mode Converter

After the electron beam travels through the cavity circuit, it is deposited on a water cooled collector wall. To keep the power per unit area low and to prevent further unwanted interaction with the electron beam, there is an uptaper region after the cavity circuit. Such a region of changing radius, however, can perform undesirable mode conversion on the extracted RF power, so the uptaper was designed to minimize mode conversion. With a nonlinear uptaper comprising a simple fillet added to the linear uptaper wall, CASCADE [15] predicted a mode purity of 99.98% for the TE_{02} mode at the center frequency of 140 GHz.

CASCADE is an advanced design code for mode analysis of two-port microwave systems based on the mode-matching technique. The fields are expanded as a series of eigenmodes that are solved by cascaded scattering matrices, producing the coupling coefficients. It can also be used to optimize complex designs in other codes, such as HFSS [16].

After the nonlinear uptaper, the TE_{02} operating mode is converted to the TE_{01} mode by a rippled wall mode converter with $N_p = 5$ periods. The number of periods was chosen based on a simple mode converter theory [17]. The following equation for the waveguide radius can be used to convert a TE_{02} mode into a TE_{01} mode, provided

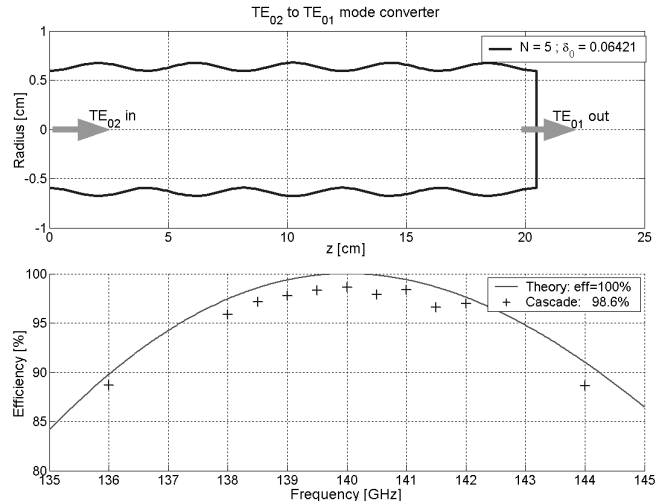


FIG. 9: The results of the lossless mode converter theory and the CASCADE code (losses included) show reasonable agreement. The mode converter consists of $N_p = 5$ periods with $\delta_0 = 0.064$ and has a bandwidth of 14 GHz and a peak efficiency of 98.6%.

the converter radius is periodic with the beat wavelength $\lambda_{B(2,1)}$ of the two modes [18],

$$a(z) = a_0 \left[1 - \delta_0 \cos\left(\frac{2\pi z}{\lambda_B}\right) \right] \quad (13)$$

where a_0 is the unperturbed cavity radius, δ_0 is the magnitude of the perturbations and

$$\Delta k_z = k_{z1} - k_{z2} = \frac{2\pi}{\lambda_B} \quad (14)$$

where the k_z 's are propagation constants for the two modes defined by,

$$k_{z1} = \sqrt{\left(\frac{\omega}{c}\right)^2 - \left(\frac{\nu_{01}}{a_0}\right)^2} \quad (15a)$$

$$k_{z2} = \sqrt{\left(\frac{\omega}{c}\right)^2 - \left(\frac{\nu_{02}}{a_0}\right)^2} \quad (15b)$$

where $J'_0(\nu_{0p}) = 0$ gives $\nu_{01} = 3.83$ and $\nu_{02} = 7.02$ for the TE_{01} and TE_{02} modes respectively.

The size of the perturbations is related to N_p by the equation,

$$\delta_0 N_p = \pi \frac{a_0^2 \sqrt{k_{z1} k_{z2}}}{\nu_{01} \nu_{02} \lambda_B} = \text{Constant} \quad (16)$$

The length $N_p \lambda_B$ of the mode converter depends on the number N_p of beat period lengths used to obtain the desired conversion efficiency. Long converters are known for inherently narrow bandwidth, but short converters may suffer from low conversion efficiency for certain mode conversion cases. In the case of TE_{02} to TE_{01} conversion,

TABLE II: MIG Design Parameters

Parameter	Value	Unit
V_0	20	kV
I_0	0.1	A
Pitch factor, α	1.5	
Beam Radius, R_b	0.64	mm
Magnetic field at cavities	5.2	T
Magnetic compression factor	40	
Cathode Radius	4.02	mm
Slant-length	0.5	mm
Current density	2	A/cm ²
Cathode slope	50	degrees
Cathode-Anode spacing factor	3	
Cathode temperature	1000	°C
Cathode roughness	64×10^{-6}	inches
Cathode position*	-55	cm
Results:		
α	1.59	
α spread	1.9	%
$\Delta v_{\perp}/v_{\perp}$ optical	0.55	%
$\Delta v_{\perp}/v_{\perp}$ thermal	1.3	%
$\Delta v_{\perp}/v_{\perp}$ roughness	4.0	%
Total velocity spread	4.2	%

(* $z=0$ is center of magnetic field)

99% conversion efficiency has been experimentally measured using only two geometrical periods ($N_p = 2$) [19].

The bandwidth of the mode converter can be evaluated by introducing a detuning parameter $\Delta\xi(\omega)$ to the definition of Δk_z in Eq. 14 as follows,

$$\Delta\xi(\omega) = k_{z1}(\omega) - k_{z2}(\omega) - \Delta k_{z0} \quad (17)$$

where Δk_{z0} is the difference of propagation constants at the design frequency and k_{z1} and k_{z2} are allowed to change simultaneously with frequency according to Eqs. 15.

The efficiency as a function of detuning is then,

$$efficiency = \left(\frac{\kappa_1(\omega)}{\kappa_2(\omega)} \sin \kappa_2(\omega) z \right)^2 \quad (18a)$$

$$\kappa_1(\omega) = \frac{1}{2} \frac{\nu_{01} \nu_{02} \delta_0}{a_0^2 \sqrt{k_{z1}(\omega) k_{z2}(\omega)}} \quad (18b)$$

$$\kappa_2(\omega) = \sqrt{\kappa_1^2(\omega) + \frac{\Delta\xi^2(\omega)}{4}} \quad (18c)$$

The ohmic losses are not taken into account in this efficiency equation as they were in the CASCADE code. This efficiency equation is plotted along with the CASCADE data points in Fig. 9.

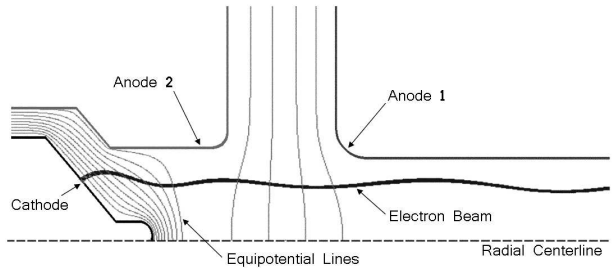


FIG. 10: Diagram of the triode MIG showing the electron beam and equipotential contours.

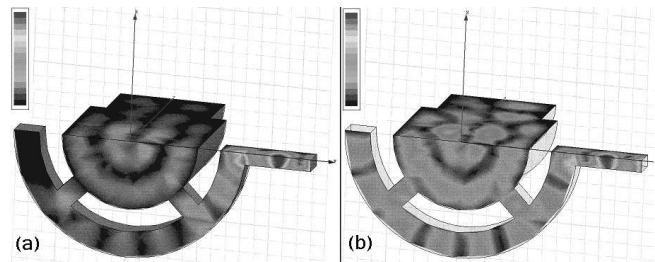


FIG. 11: The preliminary work on the input coupler (quarter-slice shown): (a) 139.4 GHz; (b) 140.3 GHz. Power enters from the right into the ring resonator modeled using standard WR6 waveguide. The power is coupled into the cavity through four coupling slots.

D. Electron Gun

The electron gun is of the Magnetron Injection Gun (MIG) type. It is responsible for creating a high quality electron beam capable of very low velocity spread. Tab. II shows all of the parameters and results of the MIG design. Since the electron gun work was performed early in the design to specify the magnet, the initial design voltage was chosen to be 20 kV instead of the final value of 15 kV. However, with the proper design adjustments, similar performance should be achievable at the final voltage of 15 kV. The optical perpendicular velocity spread of this design is unusually low at 0.55% according to the EGUN simulations [20]. The reason for this low value is that the low beam current requires only a small emitting surface, so the cathode angle is quite steep and the optical path lengths have very little spread. The largest contributor to total velocity spread is the contribution due to cathode roughness. A finer surface finish of 32 μ -inches instead of the 64 μ -inches chosen here would result in a 2.8% estimated roughness contribution instead of 4.0%. Fig. 10 shows a diagram of the triode MIG design overlaid with the electron beam and equipotential contours.

The magnet that will be used for the experiment has an anticipated $\pm 0.5\%$ homogeneity length of 28 cm and contains mild shielding such that the magnetic field falls off as $B_z(z) \sim z^{-4}$ in the vicinity of the cathode.

E. Input Coupler

Preliminary work was performed to design a suitable input coupler to get the low power RF signal into the first cavity. HFSS [16] was used to simulate a wrap-around coupler using the TE_{81} mode of a coaxial cavity with four coupling slots into the first cavity (Fig. 11). In this simple treatment, industry standard WR6 (0.065 x 0.0325 inch) rectangular waveguide was used for the input and ring resonator sections. The difficulty in designing this coupler is forming a clean TE_{02} mode inside the cavity over the frequency range of interest. The figure shows the HFSS simulations with a decent TE_{02} mode shape in the cavity at two frequencies almost 1 GHz apart. Measurements on bandwidth and coupling were not made at this time.

IV. CONCLUSIONS

The design of a wideband, 140 GHz, 100 W gyrokystron amplifier was presented. The main features of this design are an unusually low beam power of only

2.3 kW, significant saturated gain of 36 dB, and a wide bandwidth of over 1 GHz (0.75%). Linear theory was introduced as a starting point for this design. The cavity optimization procedure used was to maximize the electric fields predicted by MAGY following the direction of the electron beam traversal from the input cavity to the output cavity. This method tended to result in narrow bandwidth and over-saturation, so stagger tuning was employed to broadband the device. The specifications for the design were met by applying this stagger tuning and by increasing the cavity ohmic Q -factors and lengths as well as the drift space lengths to increase the gain.

A nonlinear uptaper section and a TE_{02} to TE_{01} mode converter were designed for high mode purity over the frequency range of interest. The mode conversion purity is above 98% over this frequency range, as predicted by CASCADE. The electron gun design yielded a predicted value of 0.55% optical perpendicular velocity spread according to EGUN for a 20 kV gun. The velocity spread due to cathode roughness is predicted to be the largest contributor to total spread. The input coupler preliminary design looks promising, although much work remains to be done on the input coupler for the TE_{02} mode.

-
- [1] A. Abragam and M. Borghini, *Progress in Low-Temperature Physics*, vol. 4. North Holland Publ. Co., 1964.
- [2] R. A. Wind, et al., "Applications of dynamic nuclear polarization in ^{13}C NMR in solids," *Progress NMR spectroscopy*, vol. 17, pp. 33–67, 1985.
- [3] K. R. Chu, H. Y. Chen, C. L. Hung, T. H. Chang, L. R. Barnett, S. H. Chen, and T. T. Yang, "Ultrahigh gain gyrotron traveling-wave amplifier," *Phys. Rev. Lett.*, vol. 81, pp. 4760–4763, 1998.
- [4] Y. Y. Lau, K. R. Chu, L. R. Barnett, and V. L. Granatstein, "Gyrotron travelling wave amplifier: I. Analysis of oscillations," *Int. J. Infrared Millimeter Waves*, vol. 2, pp. 373–393, 1981.
- [5] G. S. Nusinovich, B. Levush, and B. Danly, "Theory of multi-beam stagger-tuned gyrokystrons," *IEEE Transactions on Plasma Science*, vol. 26, pp. 475–481, 1998.
- [6] M. Blank, B. G. Danly, B. Levush, and D. E. Pershing, "Design of a 80 kW, 700 MHz bandwidth W-band gyrokystron amplifier circuit," *IEEE International Conference on Plasma Science*, p. 219ff, 1997.
- [7] M. Blank, B. G. Danly, B. Levush, and D. E. Pershing, "Experimental investigation of W-band (93 GHz) gyrokystron amplifiers," *IEEE Transactions on Plasma Science*, vol. 26, pp. 409–415, 1998.
- [8] W. Lawson, P. E. Latham, V. Specht, M. K. E. Lee, Q. Qian, J. P. Calame, B. Hogan, V. L. Granatstein, M. Reiser, and C. D. Striffler, "The design of a 100 MW, Ku band second harmonic gyro-kystron experiment," *IEEE Transactions on Plasma Science*, vol. 22, pp. 804–817, 1994.
- [9] M. E. Read, G. S. Nusinovich, M. Walter, and M. Kremer, "1 kW, 360 GHz gyrokystron," *IVEC 2000, conference abstracts, Monterey, California*, 2000.
- [10] W. Lawson, "Frequency scaling of high power gyrokystron systems," *Int. J. Infrared and Millimeter Waves*, pp. 109–110, 2000.
- [11] T. M. Tran, B. G. Danly, K. E. Kreischer, J. B. Schutkeker, and R. J. Temkin, "Optimization of gyrokystron efficiency," *Physics of Fluids*, vol. 29, no. 4, pp. 1274–1281, 1986.
- [12] V. A. Flyagin, A. L. Gol'denberg, and G. S. Nusinovich, *Infrared and Millimeter Waves*, vol. 11, pp. 179–226, 1984.
- [13] M. Botton and T. M. Antonsen, Jr., "MAGY: A time-dependent code for simulation of slow and fast microwave sources," *IEEE Transactions on Plasma Science*, vol. 26, no. 3, pp. 882–892, 1998.
- [14] G. S. Nusinovich, B. Levush, and B. Danly, "Gain and bandwidth in stagger-tuned gyrokystrons and gyrotwistrons," *IEEE Transactions on Plasma Science*, vol. 27, no. 2, pp. 422–428, 1999.
- [15] CASCADE. Cascade engine V1.60, Calabazas Creek Research, Inc., Saratoga, CA, 2001.
- [16] High Frequency Structure Simulator (HFSS). Version 9.1, Ansoft Corporation, Pittsburg, PA, 2003.
- [17] M. A. Shapiro, Private communication.
- [18] B. Z. Katsenelenbaum, L. Mercer del Rio, M. Pereyaslavets, M. Sorolla Ayza, and M. Thumm, *Theory of Nonuniform Waveguides*. London: Institution of Electrical Engineers, 1998. and references therein.
- [19] M. Thumm, "High power mode conversion for linearly polarized HE(1,1) hybrid mode output," *Int. J. Electron.*, vol. 61, pp. 1135–1153, 1986.
- [20] W. B. Hermansfeldt, "EGUN - an electron optics and gun design program," Technical report SLAC-331, UC-28, Stanford Linear Accelerator Center, October 1988.